Typeset with jjap2.cls <ver.1.0> **Regular Paper**

Measurements of Gain Spectra over Wide Spectral Ranges in GaInAsP/InP Multiple-Quantum-Well Laser Diodes

Satoshi INADA[1*], Moto KINOSHITA[1†], Masahiro YOSHITA[1], Hidefumi AKIYAMA[1], Liming ZHANG[2]

[1]*Institute for Solid State Physics, University of Tokyo, and CREST, JST, 5-1-5 Kashiwanoha, Kashiwa, Chiba 277-8581, Japan*

[2]*Bell Laboratories, Alcatel Lucent, 791 Holmdel-Keyport Road, Holmdel, New Jersey 07733, USA*

The gain spectra of 1500-nm-wavelength GaInAsP/InP multiple-quantum-well laser diodes were obtained over wide ranges of wavelength and injection current. To cover wide spectral ranges, we combined the gain spectra derived from the amplified spontaneous emission (ASE) spectra and the white-light transmittance spectra. In addition, gain (absorption) spectra for very low injection currents were obtained through ASE measurements using a liquid-nitrogen-cooled InGaAs photodiode array detector with high sensitivity. From these gain spectra, accurate estimations of the material gain and carrier-density-dependent internal loss as well as the material-transparency current were demonstrated.

KEYWORDS: quantum wells, semiconductor laser, Fabry-Pérot laser, GaInAsP/InP, gain spectrum, internal loss, transparency current

1. Introduction

Gain spectra in semiconductors are essential to understand laser performances, design various applications, and study the fundamental physics of light-matter interactions. In particular, measurements of gain spectra over wide spectral ranges are important in order to characterize the material gain and internal loss separately.[1]

A widely used gain measurement technique is the Hakki-Paoli method, which derives the gain from the Fabry-Pérot (F-P) modulation depth of the amplified spontaneous emission (ASE) spectrum below the threshold.[2] Cassidy modified this method and derived the gain by using the ratio of the integral of the wavelength-resolved power over one mode to the minimum power instead of the peak-to-valley ratio.[3] This method is much less limited by the spectral resolution of measurement systems and can be extended to measurements above the threshold.

However, there are problems with these methods: there are almost no ASE signals in the wavelength very far from the bandgap, and the ASE signals below the threshold are very weak. Because of these problems, (i) gain spectra are obtained only in limited spectral ranges around the gain peak and for limited injection-current ranges below the threshold and (ii) measurements at a wavelength of 1500 nm made using an optical spectrum analyzer (OSA) take a long time to accumulate data.

In this work, we measured gain spectra in a 1500-nm-wavelength GaInAsP/InP multiple-quantum-

*E-mail address: isatoshi@issp.u-tokyo.ac.jp

†Present address: National Metrology Institute of Japan, National Institute of Advanced Industrial Science and Technology

well (MQW) laser diode (LD) over wide ranges of wavelength and injection current and estimated the peak material gain, carrier-density-dependent internal loss, and material transparency current. To cover the wide spectral ranges, we developed experimental systems to measure ASE spectra near the bandgap and white-light transmittance spectra in wavelengths much longer than the bandgap. For ASE spectrum measurements, we prepared experimental setups that introduce a spectrometer with a liquid-nitrogen-cooled sensitive InGaAs photodiode array detector, or an optical multichannel analyzer (OMA). When different methodologies were available, we confirmed the coincidence between the results obtained by the different methods and clarified the advantages and disadvantages of each technique.

2. Principles

In the Cassidy method, the net modal gain g_{net} is given by

$$g_{\mathrm{net}} = \frac{1}{L}\ln\left(\frac{p-1}{p+1}\right), \tag{1}$$

where p is the ratio of the average mode intensity to the valley intensity of the F-P modulation in the measured ASE and L is the cavity length. The net modal gain spectra can be obtained from each value of the net modal gain g_{net} at the measured wavelength.

The net modal gain g_{net} can be decomposed as

$$g_{\mathrm{net}} = g_{\mathrm{mod}} - \alpha_{\mathrm{mirror}}, \tag{2}$$

where g_{mod} is the modal gain and α_{mirror} is the mirror loss. Because the peak net modal gain g_{net} is equal to zero in the lasing condition, the peak modal gain g_{mod} at the lasing threshold matches the mirror loss α_{mirror}. If we assume that both facets have equal mirror reflectivity R, the mirror loss α_{mirror} is given by

$$\alpha_{\mathrm{mirror}} = \frac{1}{L}\ln\left(\frac{1}{R}\right), \tag{3}$$

This quantity can be considered to be approximately constant with respect to the wavelength. Therefore, we can derive the modal gain spectra by adding the constant mirror loss α_{mirror} to the net modal gain spectra. In this paper, we assume $R = 0.3$, which is widely used for the as-cleaved facet of the conventional GaInAsP/InP MQW LDs.[4]

The modal gain g_{mod} consists of the material gain g and the internal loss α_{int}:

$$g_{\mathrm{mod}} = \Gamma \cdot g - \alpha_{\mathrm{int}}, \tag{4}$$

where Γ is the optical confinement factor of the active layer. Both the material gain g and the internal loss α_{int} depend on the carrier density in the active region and the environment. Since the internal loss α_{int} is approximately constant with respect to the wavelength, we can estimate it from the modal gain g_{mod} at wavelengths much longer than the bandgap where the material gain g can be considered to be sufficiently small.[1] Moreover, if the internal loss α_{int} is estimated, we can also estimate the material gain g for each carrier density by subtracting the constant internal loss α_{int} from the measured modal

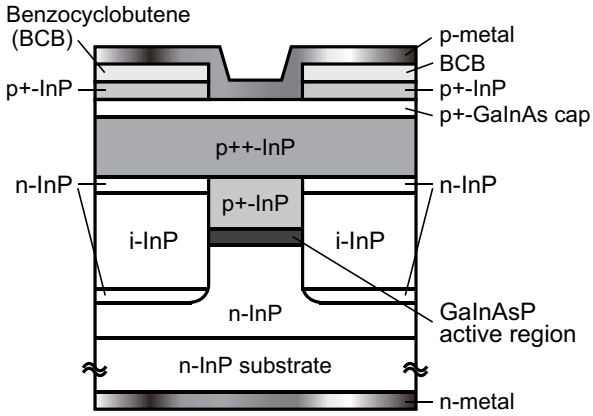

Fig. 1. Schematic cross-sectional structure of the GaInAsP/InP MQW LD.

gain. Therefore, efficient systems for measuring the ASE spectra and transmittance spectra below the bandgap are necessary for accurate estimation of the internal loss α_{int} and the material gain g for each carrier density.

3. Sample

The sample used in the experiments was a GaInAsP/InP MQW LD with a buried heterostructure using Fe-doped semi-insulating InP (i-InP), as shown in Fig. 1. The fabrication of the device involved three-step metal-organic vapor-phase-epitaxy (MOVPE) growth and photolithography. The first low-pressure MOVPE growth included the MQW region, consisting of 11 periods of 8 nm GaInAsP wells having a bandgap of 1525 nm with a strain of 0.75% and GaInAsP barrier layers having a bandgap of 1300 nm with a strain of −0.25%. The MQW waveguide was not intentionally doped, but sandwiched between n- and p-type InP confinement layers. Details of the first-growth structure of the sample are described elsewhere.[5]

After defining 5-μm-wide SiO_2 stripes, we carried out wet etching using HCl : HBr : HAc : H_2O_2. The etching depth was approximately 2.5 μm and the width of the resulting waveguide was approximately 2 μm. Then, atmospheric-pressure MOVPE growth of Si-doped n-InP and i-InP was performed. After removing the SiO_2, we finally grew the remaining p-InP cladding, p-GaInAsP contact, and p-InP cap by the third MOVPE step. Contact metals of AuBe/Ti/Au and Ti/Pt/Au were deposited and annealed on the p- and n-type sides, respectively. The two as-cleaved facets, one on each side of the waveguide, formed a F-P cavity with a cavity length of 300 μm.

The I-V and I-L characteristics of the sample in CW operation at room temperature are shown in Fig. 2. The threshold current I_{th} was about 38 mA. The lasing wavelength was 1475 nm. The external quantum efficiency η_{d} was about 27%.

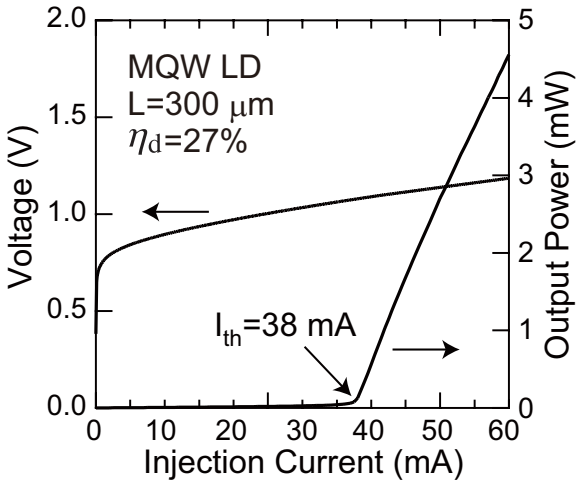

Fig. 2. Voltage and light output power versus injection current of the GaInAsP/InP MQW LD with a cavity length L = 300 μm in the CW operation mode at room temperature.

4. Experimental Setups

The experimental setups for the ASE spectra measurements using the OMA and the OSA are shown in Fig. 3(a). The ASE from the sample was collimated by an objective lens and coupled to a single-mode fiber (SMF) via an aspheric lens collimator. In the OMA setup, the light from the SMF was collimated by lens systems for F-matching, focused onto the slit of a 0.75-m spectrometer (Acton, SpectraPro-750i), dispersed therein by a 300-grooves/mm diffraction grating, and detected by a liquid-nitrogen-cooled InGaAs photodiode array detector (Roper Scientific, OMA V). In the OSA setup, the light from the SMF was fed to the input connector of an OSA (ANDO, AQ6317B). The ASE with TE linear polarization was selectively measured using a Glan-laser polarizing prism.

The setup for the transmission measurement is shown in Fig. 3(b). An ultrawideband white-light source (Santec, UWS-1000) based on a fiber laser with supercontinuum light generation was used. To cut the short-wavelength light above the bandgap energy, a longpass filter with a cut-off wavelength of 1500 nm was inserted after the collimator lenses. This probe white-light was then focused onto the laser cavity facet by an objective lens. The light transmitted from the other cavity facet was collimated via an objective lens, coupled via aspheric lens collimators into an SMF, and fed to the input connector of the OSA. In this measurement, the intensity of the probe light was so strong that data accumulation did not take a long time, even when the OSA was used for detection. After removing the sample and adjusting the focus of the objective lens, we measured the input light spectrum to obtain the transmittance spectrum. The polarizations of the probe and transmitted lights were set to TE linear polarization by means of a Glan-laser polarizing prism.

All measurements were performed at room temperature and in CW mode.

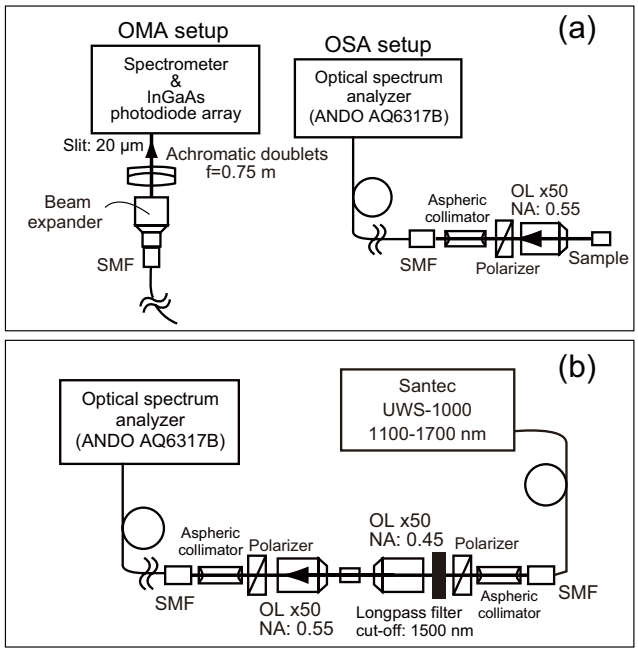

Fig. 3. (a) Experimental setups for measuring the ASE spectra using the OMA and OSA as detectors. (b) Experimental setup for measuring the transmittance spectra.

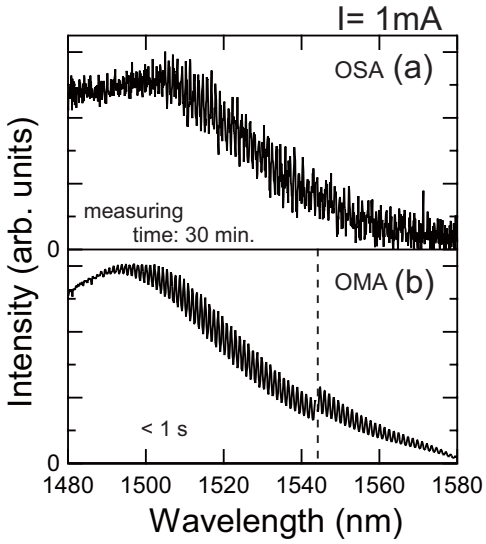

Fig. 4. Comparison of the ASE spectra obtained using (a) the OSA and (b) the OMA as a detector for $I = 0.026 \cdot I_{\mathrm{th}}$.

5. Methodology

First, we compared performances of the experimental setups using the OSA and the OMA in ASE spectrum measurements. Figure 4 shows the ASE spectra obtained using (a) the OSA and (b) the OMA for the low injection current of 1 mA, or $I = 0.026 \cdot I_{\mathrm{th}}$. We set the wavelength resolution of both the OSA and the OMA to 0.1 nm, for which gain accuracy of 1% was obtained in the Cassidy

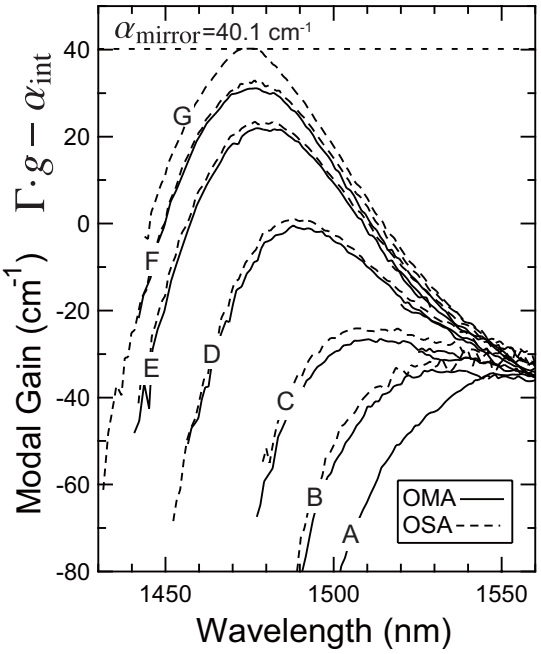

Fig. 5. Comparison of the modal gain spectra obtained by using the OMA (solid curve) and the OSA (broken curve) for various injection currents.

Table I. Injection current and measuring time for the gain spectra in Fig. 5.

Gain spectra	Injection current	Measuring time	
	(mA)	OMA (ms)	OSA (min.)
A	1	100	-
B	5	18	20
C	10	6	14
D	20	1	10
E	30	0.2	8
F	35	0.6	3
G	38	-	3

method for a cavity length of 300 μm.[6] The sensitivity of the OSA was set to the highest level. In Fig. 4(b), the broken vertical line represents the boundary of two spectra measured by changing the center wavelength of the spectrometer.

It is obvious from these figures that the ASE spectrum obtained using the OMA had a much higher signal-to-noise (S/N) ratio than that obtained using the OSA for I = 1 mA. Moreover, the measuring time was less than 1 second when using the OMA compared with about 30 minutes when using the OSA. The F-P fringe analysis was possible for only the ASE spectrum shown in Fig. 4(b) obtained using the OMA.

Next, we compared modal gain spectra derived from ASE spectra obtained using the OMA and OSA for various injection currents as shown in Fig. 5. The solid and broken curves represent the results measured with the OMA and OSA, respectively. The injection currents for curves A–G and the data accumulation times for the OMA and OSA are summarized in Table I. The broken horizontal line represents the calculated mirror loss $\alpha_{\mathrm{mirror}} = 40.1\ \mathrm{cm}^{-1}$ for $R = 0.3$ and $L = 300\ \mu$m. In Fig. 5, the gain spectra obtained using the OMA and OSA are in very good agreement. The difference of the modal gain is less than 3 cm^{-1}. For each injection current, however, the measuring time when using the OMA was much shorter than that when using the OSA, as listed in Table I. In particular, for $I = 5$ mA, it took only 18 ms with the OMA. With the OSA, it took 20 minutes about 10^5 times as long.

In Fig. 5, spectrum A for the lowest injection current was derived from the ASE spectrum shown in Fig. 4(b) obtained with the OMA. For such a low injection current, a highly sensitive OMA is indispensable. Spectrum G near the threshold current was obtained only with the OSA. In this spectrum, the F-P modulation depth in the ASE spectra was very deep. Therefore, the dynamic range of the OMA, which is about 40 dB, was insufficient. An OSA with a dynamic range of about 60 dB is suitable. These results as a whole indicate that the gain spectra obtained using the OMA and OSA are consistent, and that a high-sensitivity OMA is useful for ASE measurements while an OSA with a high dynamic range is only useful near the threshold current.

The gain spectra derived from the measured ASE spectra were limited in the wavelength region of 1450–1570 nm because of insufficient ASE intensity below this wavelength region. On the other hand, we obtained white-light transmission spectra in the wavelength region of 1520–1700 nm. To confirm the coincidence of these spectra obtained by the different techniques of ASE and transmission measurements, we compared them in the overlapping wavelength region of 1520–1570 nm, as shown in Fig. 6. The solid line and the broken line represent the results derived from the ASE spectra and the transmittance spectra, respectively, for an injection current of 30 mA. The two gain spectra show a very good overlap with the difference less than 1 cm^{-1}. We also compared gain spectra for other injection currents and found that all the results showed good agreement in the overlapping wavelength region. These results indicate that the gain spectra derived from these different techniques can be combined to form gain spectra over wide spectral ranges.

6. Gain and Internal Loss

Figure 7 shows the gain spectra derived from the ASE spectra (1430–1570 nm) and the transmittance spectra (1520–1700 nm) for various injection currents. Note that the gain spectra cover wide ranges in wavelength from 1430 to 1700 nm and in injection current from 0 mA to the threshold current ($I_{\mathrm{th}} = 38$ mA). It is obvious in the figure that spectra in the long-wavelength region show increased absorption with higher injection current. We remark here that this feature cannot be seen in spectra such as the broken curves in Fig. 5 obtained by only conventional measurements of ASE using an OSA.

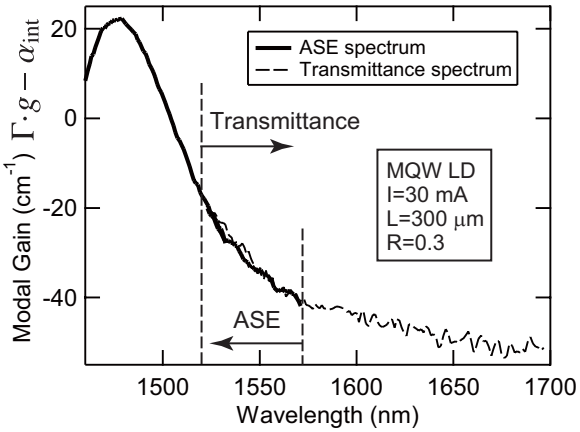

Fig. 6. Comparison of the gain spectra derived from the measured ASE spectrum (solid curve) and the transmittance spectrum (broken curve).

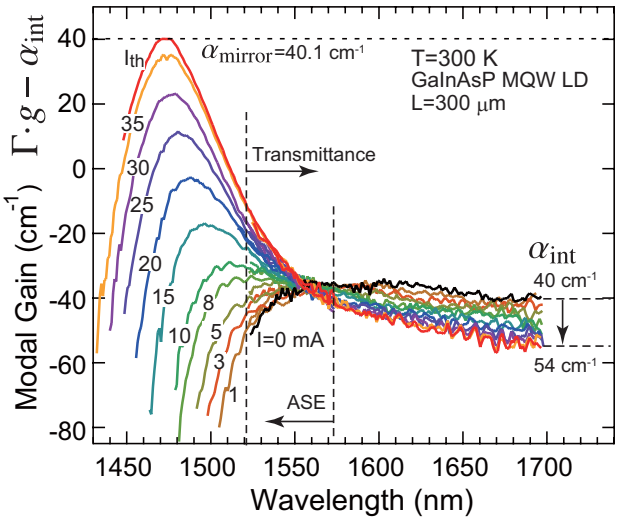

Fig. 7. Gain spectra derived from the ASE (left side) and transmittance (right side) spectra for various injection currents from 0 mA to the threshold current I_{th} = 38 mA.

Though there is a long gain tail on the long-wavelength side of a gain peak, each modal gain spectrum becomes approximately flat and is regarded as being constant in the wavelength region longer than 1670 nm. From the modal gain g_{mod} in this region, where the material gain g is considered to be sufficiently small,[1] we can estimate the internal loss α_{int}. The estimated internal loss α_{int} was 40 ± 1 cm^{-1} for zero injection current, and this increased to 54 ± 2 cm^{-1} at the threshold current I_{th} = 38 mA.

The estimated values of internal loss α_{int} determine the zero-points for the material gain g or $\Gamma \cdot g$ in the measured modal gain spectra. We would like to emphasize the importance of gain spectrum measurements over wide spectral ranges for the accurate evaluations of α_{int} and g. In fact, the gain spectra conventionally derived from only the ASE spectra in Fig. 5 or in the 1430–1570-nm region in

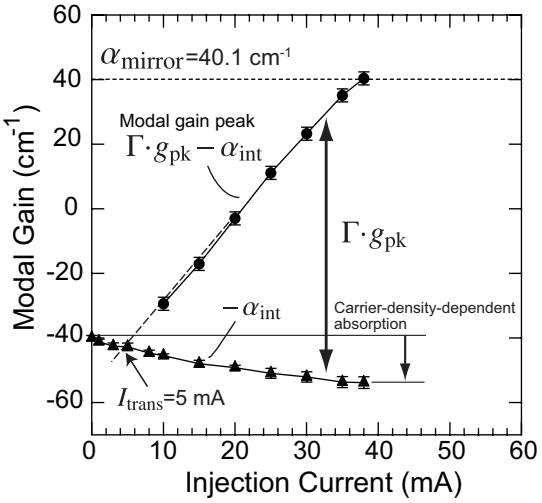

Fig. 8. Modal gain peak $\Gamma \cdot g_{pk} - \alpha_{int}$ and internal loss $-\alpha_{int}$ for each injection current.

Fig. 7 appear to converge to $g_{mod} = -35$ cm^{-1} near 1560 nm, which could easily be misjudged as a constant internal loss $\alpha_{int} = 35$ cm^{-1}.

In Fig. 7, the evolution of gain peak was clearly monitored for all injection currents from zero to the threshold current. It is known that, at the threshold current, the net modal gain should approach zero, so the modal gain g_{mod} should approach the mirror loss α_{mirror} according to eq. (2). The broken horizontal line in Figs. 7 and 8 represents the calculated mirror loss $\alpha_{mirror} = 40.1$ cm^{-1} for $R = 0.3$ and $L = 300$ μm. The gain spectrum at the threshold current I_{th} touching the broken horizontal line of the calculated $\alpha_{mirror} = 40.1$ cm^{-1} confirms the self-consistency of the present experiments.

In Fig. 8, the internal loss α_{int} is plotted together with the peak modal gain $\Gamma \cdot g_{pk} - \alpha_{int}$ for each injection current. Since the difference between the modal gain peak and the internal loss α_{int} corresponds to $\Gamma \cdot g_{pk}$, these plots reveal the carrier density dependence of $\Gamma \cdot g_{pk}$. From the intersection of the modal gain peak curve (fitted by a broken line) with the internal loss α_{int} curve, we obtained the material transparency current I_{trans}, namely the transparency current for the material gain, as 5 mA.

The values of internal loss α_{int} obtained for this device, 40 ± 1 and 54 ± 2 cm^{-1}, are large, though the present experiments could not identify their microscopic mechanisms. Figure 8 indicates that the lasing threshold should be lowered to about 20 mA with the same material gain if the internal loss α_{int} is lowered to zero. External quantum efficiency η_d=27% was measured from the *I*-*L* curve of this device shown in Fig. 2. Thus, the internal loss α_{int} of 54 ± 2 cm^{-1} at the lasing threshold with the mirror loss $\alpha_{mirror} = 40.1$ cm^{-1} gives a reasonable estimation of the internal quantum efficiency η_i=61%. We know that the obtained large values of α_{int} are inherent to the present device, since smaller values of $\alpha_{int} \sim 10$ cm^{-1} were measured in other devices with different structures and lower threshold current ($I_{th} \sim 10$ mA) by using the same measurement system. The large value of optical loss may be ascribed to the waveguide scattering or/and absorption loss in all the layers of active and cladding materials partly with heavy doping that are overlaped with the optical waveguide mode in the present device.

The carrier-density-induced change in the internal loss α_{int} by 14 cm^{-1}, from 40 ± 1 to 54 ± 2 cm^{-1}, is also large. This is most likely caused by free-carrier absorption and/or inter-valence-band absorption in the active region,[7] but this should be clarified by investigating various samples as a step toward low-threshold and high-efficiency lasers.[8]

Recently, advanced many-body physics theories have been developed toward the fundamental understanding and new design of semiconductor LDs.[9] To compare theories with experimental results for modal gain spectra in practical LDs, it is indispensable to characterize the internal loss α_{int} and extract the material gain spectra, or the key parameters of the peak material gain g_{pk} against injection current, the material transparency current I_{trans}, and the gain peak energy starting from that at I_{trans}. Measurements of the gain spectra over a wide spectral range including far below the band gap and for a wide current-injection range from zero to the lasing threshold are therefore very important.

7. Summary

We measured gain spectra of a 1500-nm-wavelength GaInAsP/InP LD over wide ranges of wavelength and injection current, and demonstrated estimations of the material gain and carrier-density-dependent internal loss as well as the material-transparency current. To cover the wide spectral ranges, we developed experimental systems for measuring ASE spectra near the bandgap and white-light transmittance spectra in wavelengths much longer than the bandgap. In the measurements of ASE spectra, we used a sensitive OMA with a liquid-nitrogen-cooled sensitive InGaAs photodiode array detector as well as an OSA. The high-dynamic-range OSA was useful for measuring lasing or ASE spectra near the threshold current, whereas the sensitive OMA was advantageous for measuring ASE spectra at a low injection current.

Acknowledgments

We thank Prof. S. Arai of Tokyo Institute of Technology and Dr. Manyalibo J. Matthews for technical supports and discussions. This work was partly supported by the Ministry of Education, Culture, Sports, Science and Technology (MEXT), Japan.

References

1) L. J. P. Ketelsen: Electron. Lett. **30** (1994) 1422.
2) B. W. Hakki and T. L. Paoli: J. Appl. Phys. **46** (1975) 1299.
3) D. T. Cassidy: J. Appl. Phys. **56** (1984) 3096.
4) D. G. Revin, L. R. Wilson, D. A. Carder, J. W. Cockburn, M. J. Steer, M. Hopkinson, R. Airey, M. Garcia, C. Sirtori, Y. Rouillard, D. Barate, A. Vicet: J. Appl. Phys. **95** (2004) 7584.
5) L. Zhang, J. Sinsky, D. Van Thourhout, N. Sauer, L. Stulz, A. Adamiecki, S. Chandrasekhar: IEEE Photon. Technol. Lett. **8** (2004) 1831.
6) V. Jordan: IEE Proc.—Optelectron. **141** (1994) 13.
7) G. Fuchs, J. Hörer, A. Hangleiter, V. Härle, F. Scholz, R. W. Glew, L. Goldstein: Appl. Phys. Lett. **60** (1992) 231.
8) A. R. Adams, M. Asada, Y. Suematsu, S. Arai: Jpn. J. Appl. Phys. **19** (1980) L621.
9) W. W. Chow and S. W. Koch: *Semiconductor-Laser Fundamentals: Physics of the Gain Materials* (Springer-Verlag Berlin Heidelberg, NewYork, 1999)